PROGRESS IN COLOR, COLORANTS AND COATINGS

available online @ www.pccc.icrc.ac.ir

Progress in Color Colorants Coating 19 (2026), 329-350

Ministry of Science, Research and Technology
Institute for Color Science & Technology

Investigation of the Distribution and Placement of Metal-Organic Frameworks in Polyvinyl Alcohol/Sodium Alginate Composites and Their Effects on Adsorption Properties for Dye Removal: A Comparison of Different Synthesis Methods

J. Moradi, A. Alikhah Shirayeh, E. Aram, H. Shaki*

Department of Polymer Engineering, Faculty of Engineering, Golestan University, P.O. Box: 49138-15759, Gorgan, Iran

ARTICLE INFO

Article history:
Received: 11 June 2025
Final Revised: 22 June 2025
Accepted: 25 June 2025
Available online: 07 Jan 2026

Keywords:
Metal-organic framework
Absorption
Polyvinyl alcohol/sodium
Removal of dyes
Composite

ABSTRACT

In this work, we investigated the incorporation of metal-organic frameworks (MOFs) into polyvinyl alcohol (PVA) and sodium alginate (SA) composites, analyzing the integration of ZIF-8 into this matrix blend and the effect of its distribution and location on adsorption properties. The PVA/SA@ZIF-8 hydrogels were prepared using three synthesis methods: one-step in situ, two-step in situ, and direct mixing. Morphology, elemental distribution, and structural integrity of the composites were characterized by FESEM, EDS, FTIR, XRD, and DLS analyses. In terms of ZIF-8 integration, the two-step in-situ method yielded the most effective distribution and integration, resulting in superior adsorption capacity. We comprehensively evaluated the removal efficiency of basic violet dye under varied conditions, including hydrogel dosage, pH, temperature, initial dye concentration, and contact time. Results demonstrated that the two-step in-situ-synthesized hydrogels exhibited the best performance, achieving approximately 99 % dye removal at an optimal dosage of 20 mg, pH 12, and T = 60 °C. The maximum dye removal efficiency for this method was observed at the initial dye concentration of 5 mg/L, reaching about 69 %. Kinetic studies indicated a predominant chemisorption process (Pseudo-Second-Order $R^2 \approx 0.99$), and thermodynamic evaluation confirmed a spontaneous ($\Delta G^\circ = -3.96$ kJ/mol at T=298 K) and endothermic ($\Delta H^\circ = +21.85$ kJ/mol) adsorption. These results collectively demonstrate the great promise of engineered PVA/SA composites incorporating MOFs for use in environmental remediation and industrial processes, driving the next generation of material design for sustainability. Prog Color Colorants Coat. 19 (2026), 329-350© Institute for Color Science and Technology.

1. Introduction

The integration of metal-organic frameworks (MOFs) into biopolymer matrices has garnered significant attention in recent years due to their potential to enhance material properties, particularly in composite systems. The purpose of this study is to investigate the distribution and placement of MOFs within polyvinyl alcohol (PVA) and sodium alginate (SA) composites, focusing on how these factors influence the absorption properties of the resulting materials [1-3].

Recent research has underscored the importance of synthesis methods in determining the structural and functional characteristics of polymer-based composites. The studies have illustrated how variations in synthesis

*Corresponding author: * Hanieh_shaki@yahoo.com; h.shaki@gu.ac.ir

https://doi.org/10.30509/pccc.2025.167568.1403

techniques can affect the morphology and dispersion of MOFs, thereby influencing performance characteristics such as mechanical strength, chemical resilience, and absorption capacity [4-7]. Additionally, the interaction between MOFs and biopolymers, such as PVA and sodium alginate, may result in synergistic effects that enhance adsorption capabilities for environmental remediation and drug delivery applications [8, 9].

Zeolitic Imidazolate Framework-8 (ZIF-8) is a metal-organic framework composed of zinc ions and imidazolate linkers, forming a highly porous crystalline structure. Its unique properties, such as high surface area, thermal and chemical stability, and tunable pore size, make it suitable for a wide range of applications. Since its synthesis in 2006 [10], ZIF-8 has attracted significant attention for its exceptional stability and adjustable porosity, making it a leading adsorbent for environmental cleanup. One significant application is the removal of dyes from wastewater [11-13], where ZIF-8's large surface area and functionalizability enable effective adsorption of organic contaminants. Its ability to selectively capture and retain different dye molecules positions ZIF-8 as a promising solution for addressing water pollution and improving the sustainability of industrial processes, underscoring its importance in materials science and environmental protection [14]. As the demand for advanced materials continues to grow, analyzing the distribution of MOFs within PVA/SA composites becomes essential. Optimal mixing techniques can indeed enhance interfacial adhesion, which significantly impacts the efficiency of absorption processes. [15, 16]. Additionally, tailoring synthesis methods not only helps acquire desired physical properties but also enables the engineering of specific functionalities that cater to diverse industrial applications [17, 18].

This study presents a systematic investigation of various synthesis methods for embedding MOFs within PVA/SA composites and examines their impact on morphology and absorption properties. By synthesising insights from recent advancements in materials science and environmental engineering, this research aims to facilitate the development of innovative composite materials with improved performance. The outcomes of this investigation are expected to make significant contributions to both academic research and practical applications in material design and environmental sustainability [19-21]. Unlike previous studies [22, 23] that focused solely on either material synthesis or adsorption performance of MOF-polymer systems, this work presents a systematic comparative analysis of three distinct synthesis strategies-one-step in-situ, two-step in-situ, and direct mixing-for embedding ZIF-8 into a PVA/sodium alginate hydrogel matrix. The study uniquely correlates structural characteristics (e.g., particle size distribution, morphology, elemental dispersion) with adsorption performance, including kinetic and thermodynamic behaviors, across these synthesis methods under identical conditions. This integrated approach not only reveals how the synthesis route governs material functionality, but also identifies the two-step in-situ method as a strategically superior pathway for maximizing dye removal. To the best of our knowledge, such a comprehensive structure-performance correlation using ZIF-8 in a dual-polymer hydrogel matrix has not been reported previously.

2. Experimental

2.1. Materials

In ZIF-8 (Zeolitic Imidazolate Framework-8) synthesis, 2-methylimidazole and zinc nitrate hexahydrate 98 % were obtained from Sigma-Aldrich. Poly (vinyl alcohol), MW 30000, 98 % hydrolyzed (PVA 30K 98 %), and sodium alginate were also supplied by Sigma-Aldrich. Calcium chloride and sodium hydroxide were purchased from Merck. Hydrochloric acid 37 %, methanol 99.5 % and deionized water were all bought from Dr. Mojallali Ind. Co. (Iran). Basic violet 1 (triarylmethane color) was also purchased from Alvan Sabet Ind. Co. (Iran).

2.2. Methods

FTIR spectra were recorded using a PerkinElmer Spectrum PX-I spectrometer equipped with a deuterated triglycine sulfate (DTGS) detector. Morphological characterization was conducted using a TESCAN MIRA3 FE-SEM. Samples were cryo-fractured, sputter-coated with 10 nm Au (Denton Desk V HP), and imaged at 10 kV acceleration voltage and 7 mm working distance. Images were acquired in SE mode at 50,000 × magnification using TESCAN LYRA v5.0 software. Crystallographic characterization was performed using an ASENWARE AW-XDM300 X-ray diffractometer with Cu Kα radiation (40 kV, 30 mA). Powder samples were scanned from 5° to 80° (2θ) at a step size of 0.02° and scan speed of 2°/min. Phase

identification was conducted using the ICDD PDF-4+ database via ASENWARE XDM Analysis Suite v2.0. Elemental distribution was also analyzed using a TESCAN VEGA3 SEM with a SAMX EDS detector. Carbon-coated samples were imaged at an acceleration voltage of 20 kV and a working distance of 10 mm. EDS maps (1024 × 768 pixels, 50 µs/pixel) and spectra were acquired using AZtecLive Advanced v6.0, with quantification via ZAF correction. Optical absorption spectra were acquired using a PG Instruments T90+ spectrophotometer. Samples dissolved in DMF (1 mg/mL) were scanned from 200–800 nm at 240 nm/min scan speed with a 2 nm slit width. Baseline correction and λ_{max} determination were performed using UVWin5 v5.0.5. For dynamic light scattering (DLS) analysis, the samples were also placed in microcentrifuge tubes and suspended in deionized (DI) water. For analysis, 3 mL of the suspension was placed in a cuvette and read in a Beckman Coulter Delsa Nano C to estimate the average particle size.

2.3. Synthesis of ZIF-8 metal-organic framework

ZIF-8 was successfully synthesized by dissolving zinc nitrate hexahydrate and 2-methylimidazole in water (solutions 1 & 2, respectively). Then, Solution 1 was added to Solution 2. The mixtures were stirred at 50 °C for 6hours for the crystallization of ZIF-8. After the reaction, the ZIF-8 powder was collected by repeated centrifugation (at 5000 rpm for 20 minutes) and washed three times with methanol, then dried overnight under vacuum at 120 °C [24, 25].

2.4. Preparation methods of PVA/SA@ZIF-8 hydrogel

In this study, three different methods were used to prepare hydrogel composites containing MOF.

2.4.1. One-step in-situ preparation method

According to previous research [26, 27], 1 g of polyvinyl alcohol and 1 g of sodium alginate were mixed and dissolved in 100 mL of deionized water, then vigorously stirred for 5 hours at 80°C to obtain a homogenized, viscous solution. After cooling to room temperature while stirring, it was slowly poured into a 5 % solution of zinc nitrate hexahydrate, continuing to stir during the addition. The resulting beads were maintained in this solution for 24 hours. Next, 2-methylimidazole was dissolved in a methanol solution at a concentration of 20 mg/mL. The obtained beads were washed three times with deionized water. Subsequently, the beads were immersed in the 2-methylimidazole solution and soaked for 24 hours, followed by washing and drying in a vacuum oven at 60 °C for 6 hours.

2.4.2. Two-step in-situ preparation method

As in the previous method and that of Zhang et al. [28], 1 g of polyvinyl alcohol and 1 g of sodium alginate were mixed and dissolved in 100 mL of deionized water, then stirred vigorously at 80 °C for 5 hours to obtain a homogenized, viscous solution. After cooling to room temperature under stirring, the solution was slowly added to a methanol solution containing 40 mg/mL of zinc nitrate hexahydrate and 20 mg/mL of 2-methylimidazole, and stirred for 24 hours at room temperature. The mixture was then washed and dried in a vacuum oven at 60 °C for 6 hours.

2.4.3. Direct mixing of MOF in the hydrogel method

In the third method, 1 g of polyvinyl alcohol, 1 g of sodium alginate, and 10 mg of ZIF-8 were separately dissolved in 100 mL of deionized water, then stirred vigorously. After 1 hour of mixing, ZIF-8 was sonicated for 10 min using an ultrasonic homogenizer to ensure complete dissolution in water. Then, the solutions containing polyvinyl alcohol, sodium alginate, and ZIF-8 were combined and stirred vigorously at 80 °C for 5 hours to obtain a homogenized viscous solution. After cooling to room temperature, the mixture was slowly dripped into a 5 % calcium chloride solution while being stirred. The formed beads were kept in this solution for 24 hours. They were then washed and dried in a vacuum oven at 60 °C for 6 hours. A closely related study that employed a similar method was also conducted by Wang et al. [29]. The preparation of the PVA/SA@ZIF-8 hydrogel by all three methods is shown in Figure 1.

3. Results and Discussions

3.1. Characterization of ZIF-8 and PVA/SA@ ZIF-8

3.1.1. FESEM analysis

The FESEM images of PVA/SA@ZIF-8 are shown in Figure 2. Sample A is a sample synthesized by a one-

step in-situ method, sample B is a two-step in-situ synthesis sample, and sample C is produced by a direct mixing method. As shown in the images, the surface morphology of sample A presents a more open, less dense arrangement with a more regular structure. Also, the surface is less rough, indicating less agglomeration and higher potential porosity. Sample B exhibits a relatively rough and clustered structure. Particle sizes appear to vary significantly, indicating possible aggregation. Figure 2 C shows a heterogeneous morphology comprising densely clustered particles and interconnected fibrous networks. Quantitative analysis of FESEM images revealed that sample A exhibited a relatively uniform nanoparticle distribution, with an average particle size of 80-120 nm, indicative of well-dispersed ZIF-8 within the polymer matrix.

In contrast, sample B showed noticeable particle agglomeration and a broader size distribution from 100 to 250 nm, resulting in decreased porosity. Sample C displayed an intermediate morphology with fibrous structures and clusters, with particle sizes ranging from 90 to 200 nm, suggesting partial aggregation. These morphological characteristics directly influence the availability of active adsorption sites, thereby affecting dye removal efficiency [30].

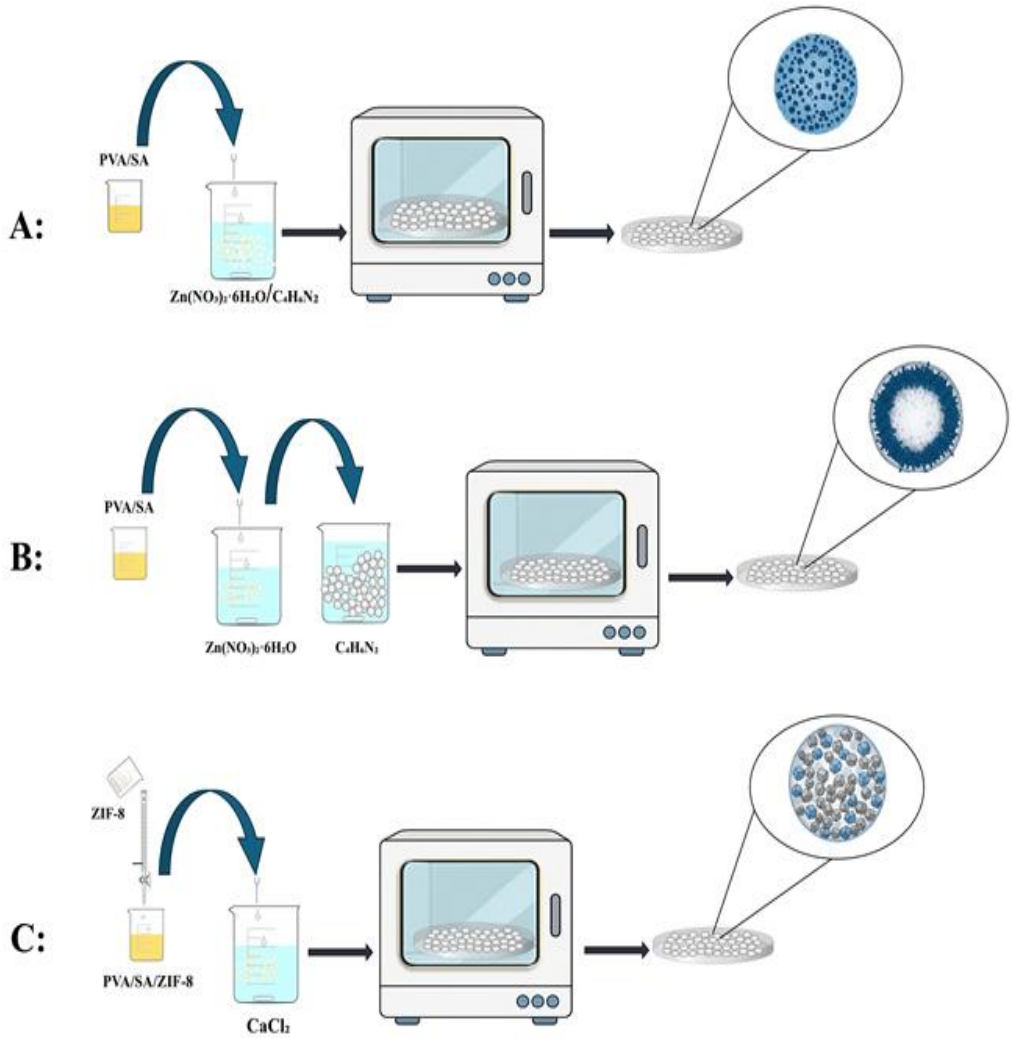

Figure 1: General schematic of the methods for preparing a hydrogel composite containing MOF.

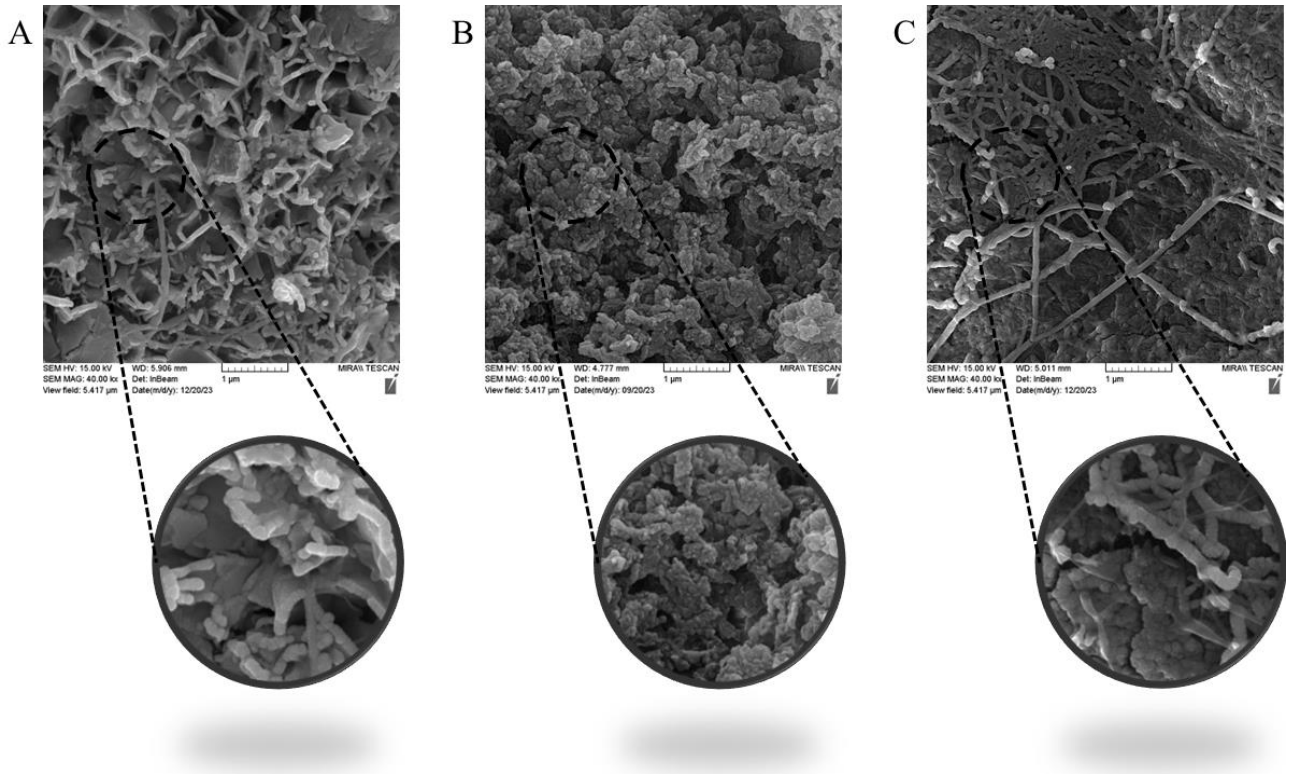

Figure 2: SEM images of PVA/SA@ZIF-8 hydrogels that were synthesized by (A) One-step in-situ preparation, (B) Two-step in-situ preparation, and (C) Direct mixing of MOF in hydrogel methods.

3.1.2. EDS map analysis

EDS provides crucial insights into the distribution and integration of ZIF-8 within the hydrogel matrix (Figure 3). Expectedly, carbon (C), oxygen (O), sodium (Na), nitrogen (N), and zinc (Zn) elements were observed across all samples, with zinc and nitrogen originating from ZIF-8 and carbon/oxygen from the polymer backbone.

Quantitatively, sample A (one-step in-situ) showed a notable zinc content of 7.31 %, along with high percentages of oxygen (32.46 %) and carbon (31.39 %). The EDS map for sample A (Figure 3A) visually confirms a high, relatively uniform distribution of zinc throughout the analyzed area, suggesting effective integration and dispersion of ZIF-8 within the polymer matrix. This optimal ZIF-8 integration is expected to directly increase accessible surface area and porosity, aligning with FESEM observations of its open structure and consequently enhancing its adsorption performance. In contrast, sample B (two-step in-situ) exhibited a significantly lower zinc content (0.13 %) in the quantitative analysis, despite its superior adsorption performance. This seemingly contradictory observation is critical: the EDS map for sample B (Figure 3B) reveals poor, localized ZIF-8 integration, suggesting its presence is concentrated on the surface of the hydrogel grains rather than uniformly dispersed throughout the bulk. This limited bulk incorporation, leading to a denser overall structure and lower apparent porosity according to FESEM, nevertheless achieves high dye removal due to highly reactive, surface-exposed ZIF-8 particles and optimized interactions that facilitate rapid adsorption kinetics. This implies that, for sample B, the "effective integration" mentioned in the abstract refers more to the quality of interfacial interactions and surface availability than to bulk uniform distribution. Sample C (direct mixing) presented the highest zinc percentage (9.27 %) among the samples, but with a lower carbon content (23.49 %) compared to sample A. The EDS map for sample C (Figure 3 C) shows a more complex, variable distribution of ZIF-8, characterized by areas of higher zinc concentration interspersed with regions of lower MOF abundance. This heterogeneous distribution correlates well with its complex morphology observed in FESEM (Figure 2 C) and suggests a balance between effective integration and potential agglomeration. This mixed integration pattern likely contributes to its moderate dye removal efficiency, falling between the performances of samples A and B.

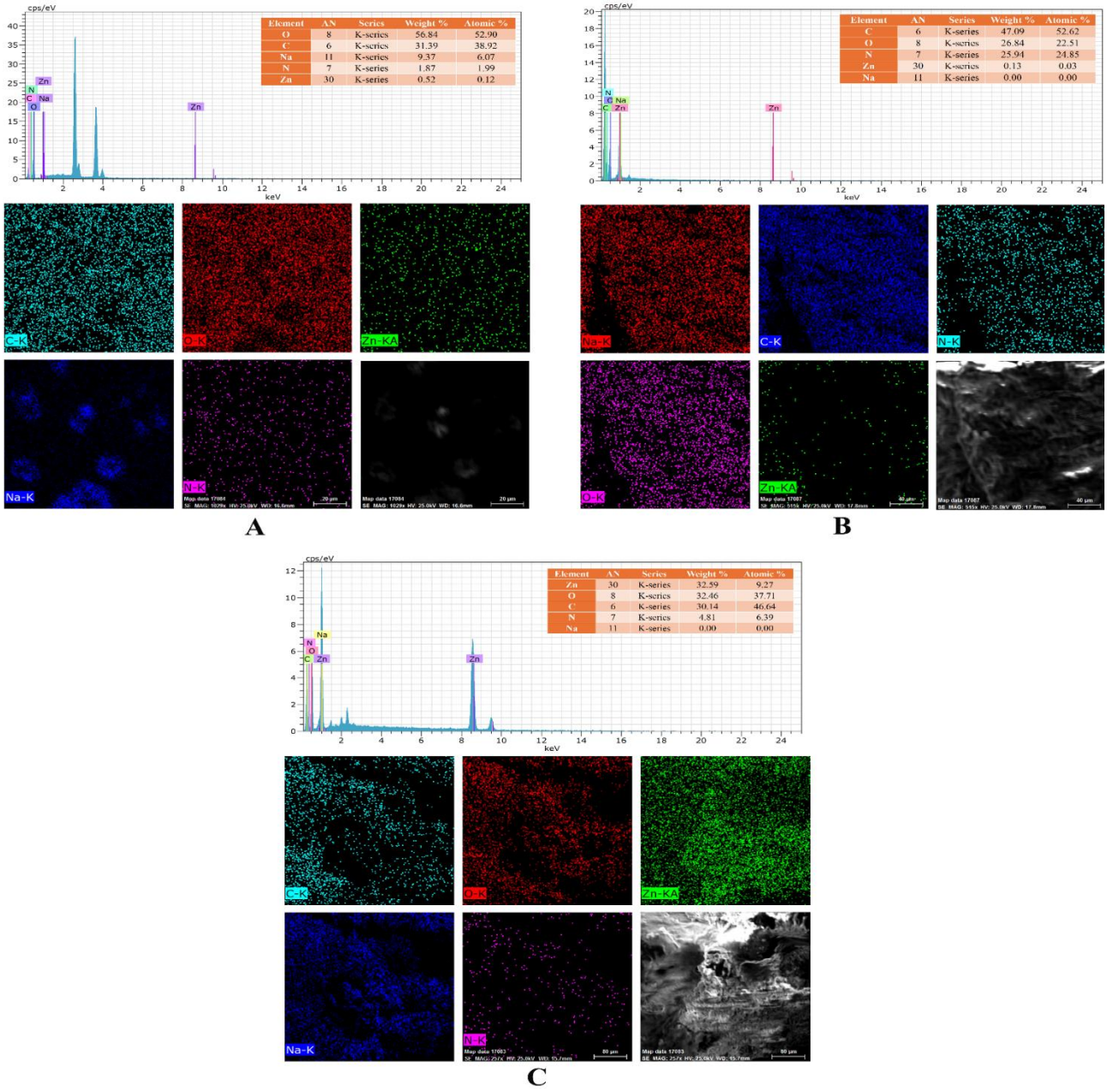

Figure 3: EDS mapping of PVA/SA@ZIF-8 hydrogels synthesized by (A) One-step in-situ preparation, (B) Two-step in-situ preparation, and (C) Direct mixing of MOF in hydrogel methods.

3.1.3. XRD analysis

The analysis of ZIF-8 X-ray diffraction (XRD) patterns will focus on three main features -peak positions, intensities, and overall pattern shape -to determine the integrity of the crystalline structure and phase purity [31]. As shown in Figure 4, the sharply defined XRD peaks indicate a crystalline structure. ZIF-8 typically exhibits high crystalline order. Notable peaks have been observed at 2θ of 7.54°, 10.64°, 12.94°, and 18.34°. According to the Crystallography Open Database, these peaks are in the correct positions, confirming the ZIF-8 synthesis. Also, based on the calculations and simulations, the mentioned peaks can be attributed to the plates with Miller indices (110), (200), (211), and (222), respectively. The peak intensities indicate the relative abundance of specific crystallographic orientations, and the low background noise indicates good crystallinity in the sample.

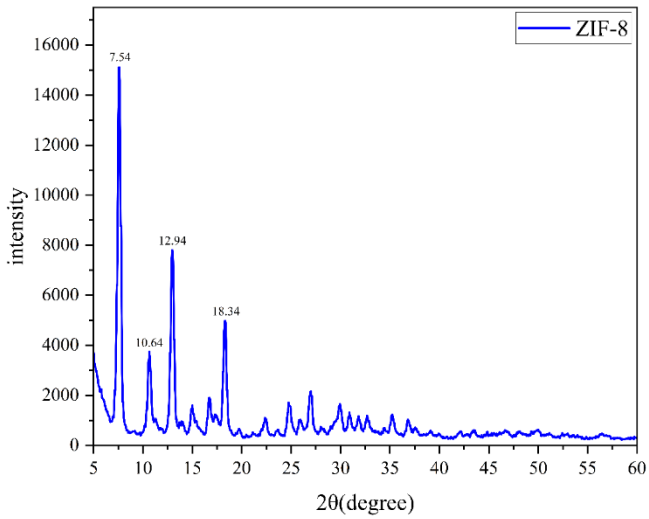

Figure 4: XRD spectra of ZIF-8 MOF.

3.1.4. Dynamic Light Scattering (DLS) analysis

Dynamic Light Scattering (DLS) analysis was used to assess the size distribution of the synthesized ZIF-8 MOF nanoparticles, which serve as the building blocks for our composites. As shown in Figure 5, DLS yields particle-size data in three weighting schemes: number (A), intensity (B), and volume (C). The number-weighted histogram (Figure 5A) clearly indicates that the majority of ZIF-8 particles are in the nanoscale range, primarily 101–102 nm, with a relatively sharp peak indicating a dominant population of small crystallites. This small size is crucial for maximizing surface area for adsorption.

However, the intensity-weighted plot (Figure 5B) shows a significant shift towards larger apparent sizes, with a pronounced feature at higher diameters (up to 500 nm). This indicates the presence of a minor fraction of larger particles or aggregates that, despite their low count, dominate the scattered light intensity due to its steep dependence on particle diameter (∝ diameter^6). The volume-weighted distribution (Figure 5 C) provides an intermediate view, confir-ming the dominant population of small particles while also highlighting the substantial contribution of the larger aggregates to the total particle volume.

Collectively, these DLS results demonstrate that the synthesized ZIF-8 sample exhibits moderate poly-dispersity, comprising a predominant population of well-formed nanocrystals alongside a small but volumetrically significant fraction of larger aggregates. This inherent size heterogeneity of the ZIF-8 precursor is important, as it can influence its dispersion and integration mechanisms within the PVA/SA matrix during different synthesis methods, potentially affecting the final composite's pore structure and, ultimately, its adsorption efficiency. In Figure 5, A, B, and C show count, intensity, and volume distribution, respectively.

3.1.5. FT-IR analysis

FTIR spectroscopy is a valuable tool for charac-terizing the structural quality of synthesized ZIF-8 metal-organic frameworks (MOFs). The FTIR spectrum in Figure 6A exhibits distinct vibrational bands that represent all functional groups found in the ZIF-8 structure. The O-H stretching vibrations in infrared (IR) spectroscopy are indeed associated with a broad absorption band near 3400 cm^{-1}, primarily due to the presence of hydroxyl groups and moisture. The imidazole linker exhibits two intense absorption peaks at 3134 and 2920 cm^{-1}, which reflect aromatic C–H stretching of the imidazole functionality and aliphatic C–H stretching of the 2-methylimidazole ligand, respectively. The strong peak at 2342 cm^{-1} in the spectrum indicates the presence of C-N stretching vibrations, which are characteristic of the imidazolate linker units within a framework structure. The C=N stretching vibration of the imidazole ring can be found at 1585 cm^{-1} and the C–H bending vibrations of the methyl group in 2-methylimidazole occur at 1460 cm^{-1}. The peaks in the FTIR spectrum of ZIF-8 indicate the successful formation of the metal-organic framework, highlighting the presence of imidazole ligands and metal coordination features. These results have been replicated in various studies that have similarly synthesized ZIF-8, including Hao et al. [32].

The FTIR spectrum in Figure 6B corresponds to the PVA/SA@ZIF-8 hydrogel synthesized via a single-step in situ method. The 3420 cm^{-1} peak in an infrared spectrum is indeed indicative of O-H stretching vibrations, which are characteristic of the presence of hydroxyl groups (-OH). These vibrations are commonly observed in both polyvinyl alcohol (PVA) and sodium alginate (SA), due to the hydroxyl groups present in their molecular structures. The 2925 cm^{-1} peak corresponds to C-H stretching vibrations of methylene ($-CH_2$) groups, present in both PVA and SA structures. The peak at 1636 cm^{-1} is typically associated with C=O bending vibrations, indicating the presence of a carbonyl group. This may arise from

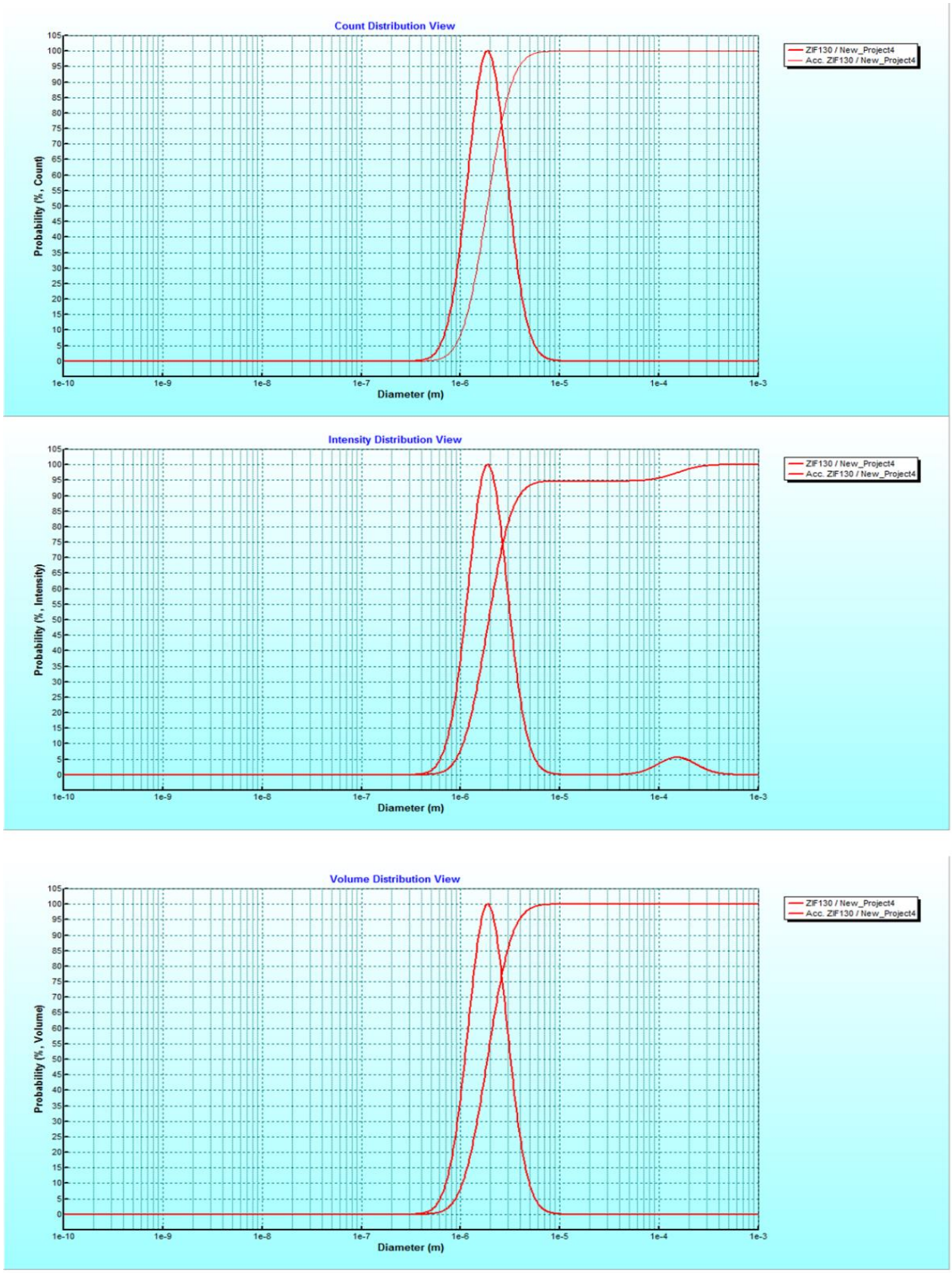

Figure 5: DLS spectra of (A) number, (B) intensity, and (C) volume of ZIF-8 MOF.

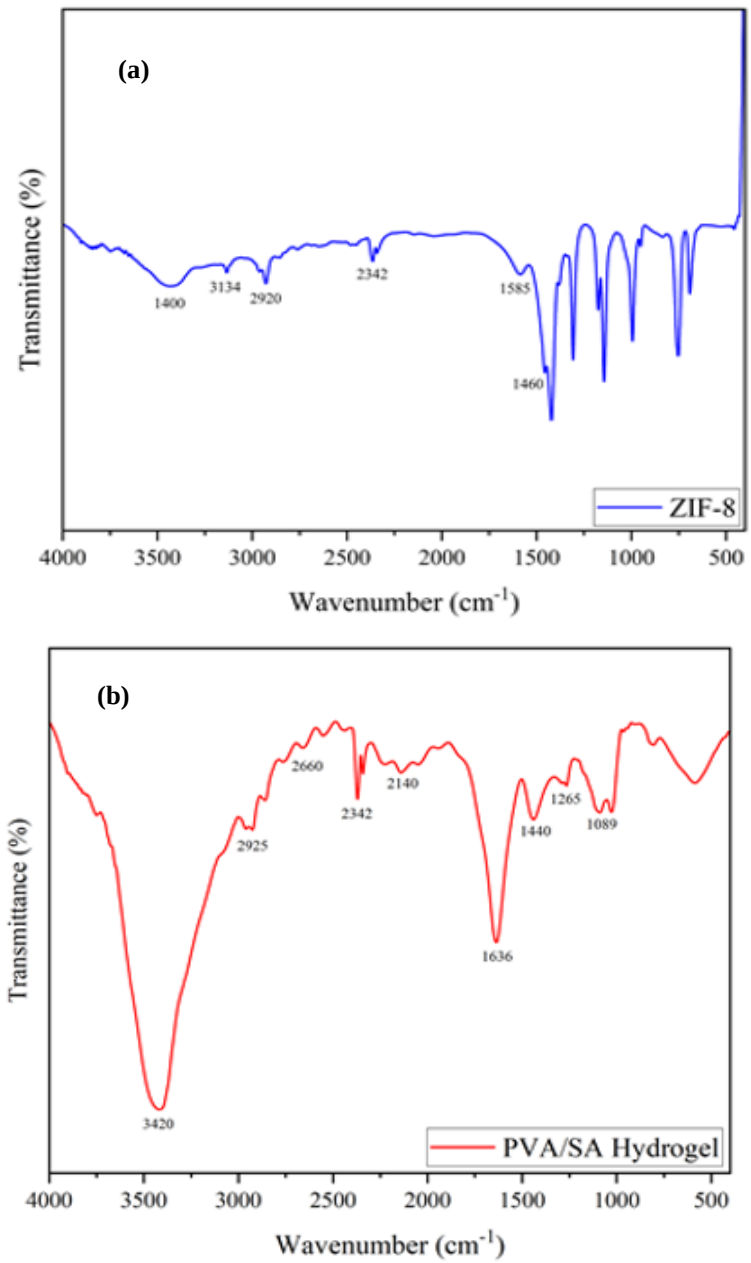

Figure 6: FTIR spectra of (a) ZIF-8 MOF and (b) PVA/SA hydrogels.

the degradation of polymer chains. The presence of a band at 1439 cm^{-1}, indicative of C-H bending vibrations, particularly from CH_2 and CH groups, is a strong indicator of both PVA and SA. The observed peak at 1265 cm^{-1} often corresponds to C-O stretching in the polysaccharide portion, particularly in SA. The presence of specific peaks in the FTIR spectra corresponding to known functional groups in PVA and SA confirms that the hydrogel is indeed composed of these two polymers. Moreover, a shift in the O–H stretching peak from 3420 to 3390 cm^{-1} was observed in the composite spectrum, suggesting the formation of hydrogen bonding between ZIF-8 and hydroxyl groups in PVA and SA. Additionally, the emergence of a new band at approximately 1265 cm^{-1} is attributed to C–O–Zn stretching vibrations, confirming the successful chemical interaction between the polymer matrix and the metal center in ZIF-8. These spectral changes support the effective incorporation of MOF into the polymeric network at the molecular level, thereby enhancing both structural stability and adsorption functionality [33].

3.2. Absorption optimization and performance

3.2.1. Effects of the PVASA@ZIF-8 bead dose on removal efficiency

To investigate the removal efficiency at different doses of PVA/SA@ZIF-8 hydrogel beads, specific amounts of 0.005, 0.01, 0.02, 0.05, 0.075, and 0.1 g of these hydrogel beads were stirred in 20 mL of Basic Violet dye solution with a concentration of 10 mg/L for 90 min at room temperature [34].

Different amounts of PVA/SA@ZIF-8 hydrogel beads were added to 20 mL of Basic Violet solution at 10 mg/L. The applied temperature was 20°C, with a pH of 12. The effect of adsorbent dosage on the removal efficiency of Basic Violet dye was systematically examined by varying the dose of PVA/SA@ZIF-8 composite beads from 5 to 100 mg. The corresponding results are illustrated in Figure 7A-C.

In all three systems, an overall increase in dye removal efficiency was observed with increasing adsorbent dosage, particularly at lower doses (5-20 mg). The initial increase in dye removal efficiency during adsorption is primarily due to the greater availability of active sites and a larger surface area for the dye molecules to interact with the adsorbent. When an adsorbent is used to remove substances from a solution, its effectiveness initially increases with dosage, but beyond a certain point, the removal efficiency plateaus or even slightly decreases. This phenomenon is often attributed to either mass transfer limitations, in which the rate of substance reaching the adsorbent's surface is slower than the reaction rate, or to particle aggregation, in which adsorbent particles clump together, reducing the available surface area for binding. In sample A, the removal efficiency improved sharply from 67 % at 5 mg to approximately 87 % at 20 mg, then declined slightly before rising to 93 % at 100 mg. The non-linear trend beyond 20 mg suggests a possible redistribution of dye molecules across excess adsorption sites or shielding effects due to bead clustering.

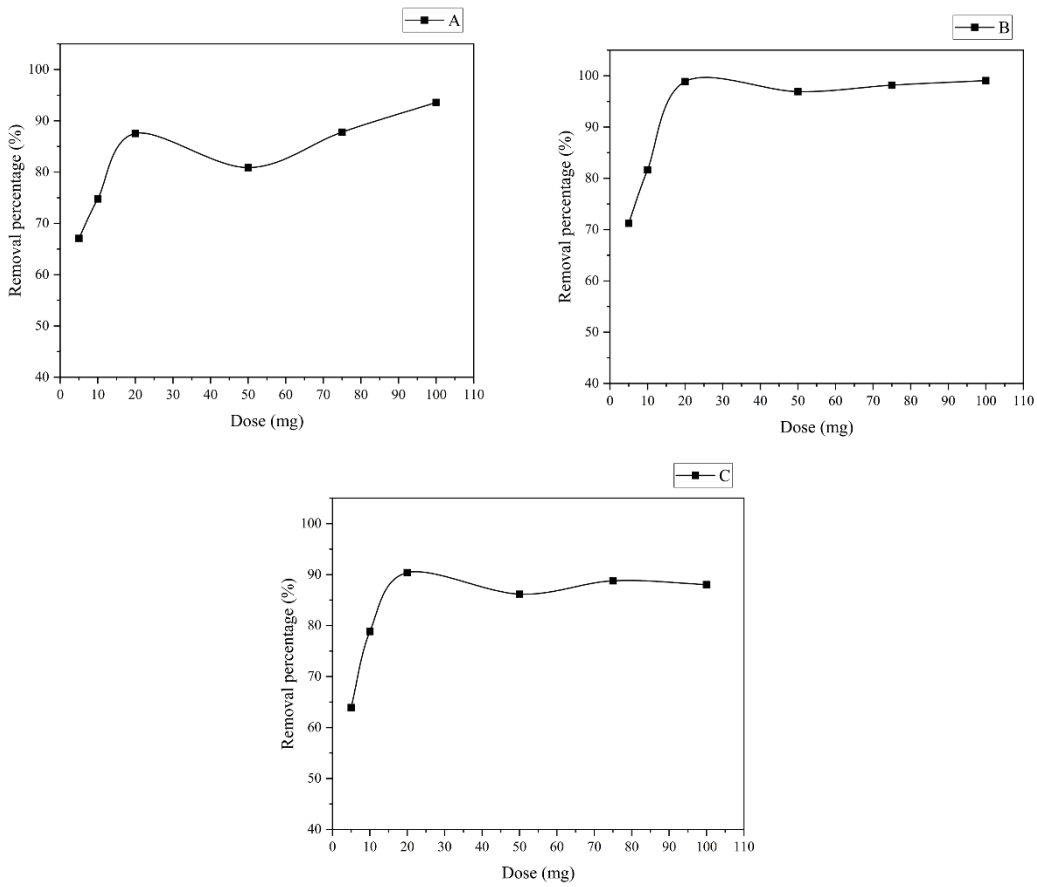

Figure 7: Effect of PVA/SA@ZIF-8 bead dosage on the removal curve of PVA/SA@ZIF-8 hydrogels synthesized using (A) one-step in-situ preparation, (B) two-step in-situ preparation, and (C) direct mixing of MOF into the hydrogel.

Sample B exhibited the most efficient dye removal performance, achieving near-complete removal (~99 %) at 20 mg and maintaining this high efficiency across the entire dosage range. This superior behavior may reflect favorable dye-bead interactions, high surface affinity, and minimal mass transfer resistance under the tested conditions.

Sample C showed a trend similar to that of system A, with removal efficiency increasing from 64 % at 5 mg to about 90 % at 20 mg. After this stage, a slight decline, followed by stabilization at 88-89 %, was observed up to 100 mg. This behavior may result from surface saturation or the formation of a concentration gradient that limits the diffusion of dye molecules into the bead matrix.

Collectively, these findings underscore that while increasing the dosage of PVA/SA@ZIF-8 beads generally enhances basic violet dye removal, the benefit diminishes at higher dosages due to kinetic and equilibrium constraints. Thus, identifying an optimal adsorbent dose is critical to achieving high removal efficiency without unnecessary material consumption or compromised performance.

3.2.2. Effect of the initial pH on removal efficiency

The removal efficiency of basic violet dye under different pH conditions was evaluated by stirring 0.02 g of PVA/SA@ZIF-8 hydrogel beads in 20 mL of a basic violet dye solution (10 mg/L) for 90 min at room temperature. For this purpose, pHs were adjusted to 4, 7, 9, 11, and 12. The removal efficiency of Basic Violet dye in various pH levels is illustrated in Figure 8A–C.

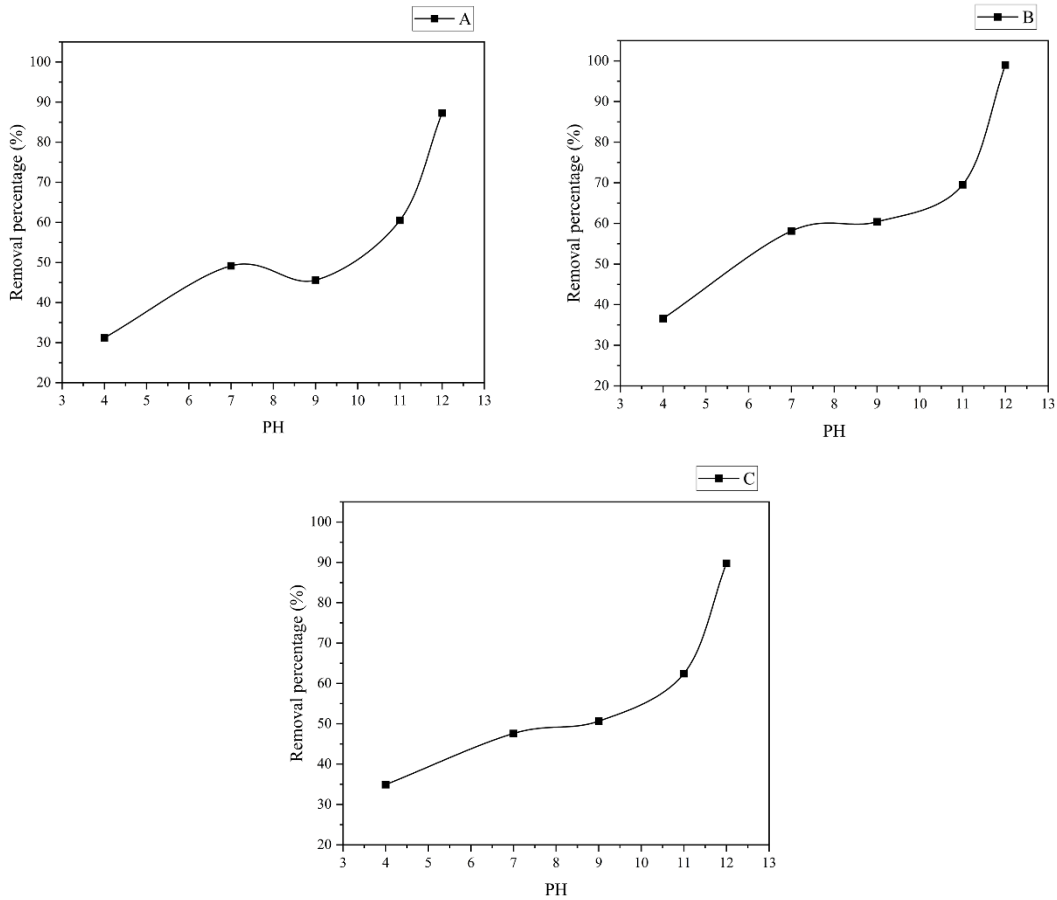

Figure 8: Effect of pH on the removal curve of PVA/SA@ZIF-8 hydrogels synthesized using (A) one-step in-situ preparation, (B) two-step in-situ preparation, and (C) direct mixing of MOF into the hydrogel.

In the one-step in-situ method (A), the removal efficiency of the basic violet 16 dye increases with increasing pH from acidic to alkaline conditions. At low pH (pH=3-5), removal efficiency ranges from 30-45 %, attributed to the protonation of functional groups such as carboxyl in SA and imidazole in ZIF-8, which results in a positively charged adsorbent surface and electrostatic repulsion with the cationic dye. At neutral pH (pH=7), a slight decrease to approximately 50 % is observed, likely due to proximity to the point of zero charge (pHpzc), which minimizes electrostatic interactions. In alkaline conditions (pH = 8-12), the removal efficiency sharply increases, reaching ~95 % at pH 12, attributed to the deprotonation of negative sites, which enhances electrostatic attraction, π-π interactions, and physical adsorption within ZIF-8 pores, supported by the high structural stability provided by in-situ integration.

In the two-step in-situ method (B), the removal curve for basic violet 16 is continuous and sigmoidal, showing a steady increase from acidic to alkaline pH. At pH 3-5, the removal efficiency is 35-40 %, slightly higher than that of method A, due to the increased stability of ZIF-8 within a PVA/SA network under acidic conditions. In the pH range 6-8, removal reaches 45-60 % without significant fluctuations, indicating uniform MOF distribution and interaction with hydrophilic PVA. At pH = 9-12, the increase becomes steeper, achieving 95 % at pH = 12, where dominant mechanisms include electrostatic binding to $-COO^-$ sites and coordination with ZIF-8, alongside reduced competition from hydrogen ions.

In the direct mixing method (C), removal efficiency is lower than that of in-situ methods and shows an initial decline under acidic conditions. At pH 3-5, efficiency drops from 30 to ~20 %, due to ZIF-8 aggregation, reduced effective surface area, and increased electrostatic repulsion with the cationic dye. In the pH 6-8 range, a gradual improvement to 25-40 % is observed, but performance remains inferior to other methods, likely due to poor interfacial integration and greater susceptibility to protonation. At pH= 9-12, removal increases linearly, reaching a maximum of 80 % at pH 12, driven by activated electrostatic and physical interactions, though structural limitations prevent higher efficiency.

In conclusion, in-situ methods (A & B) achieve ~95 % removal efficiency at pH 12, significantly outperforming the direct mixing method (80 %), owing to better ZIF-8 distribution and structural stability under alkaline conditions. The optimal pH for all methods is above 9, where the negative surface charge maximizes cationic dye adsorption, while acidic pH limits efficiency due to repulsion and degradation.

3.2.3. Effect of the temperature on removal efficiency

To investigate the effect of temperature on the removal efficiency of basic violet dye, 20 mg of PVA/SA@ZIF-8 hydrogel was stirred in 20 mL of a 10 mg/L basic violet solution at various temperatures (10, 20, 30, 40, 50, and 60 °C) for 90 min, maintaining a constant pH of 12.

Figure 9A shows that the composite material maintains a consistently high removal efficiency of around 95 % across a wide temperature range from 0 to 60 °C. This suggests that temperature change has a minimal impact on the material's removal performance.

Figure 9B shows a positive correlation between temperature and dye removal efficiency, with a rise in temperature from lower values to 60 °C corresponding to an increase in removal percentage from approximately 85 % to nearly 90 %. This finding shows that the composite material's active sites or interactions with the dye become more efficient at higher temperatures, thereby improving removal.

Figure 9 C demonstrates a notable increase in the percentage of dye removal as the temperature rises. The removal efficiency jumps from approximately 75 % at 0 °C to over 90 % at 60 °C, indicating a clear positive relationship between temperature and dye removal efficiency. This finding shows that the interaction between PVA/SA@ZIF-8 and the basic violet dye increases at higher temperatures, potentially due to higher diffusion rates or more favorable interactions driven by increased thermal energy.

The overall trend indicates that temperature influences the removal efficiency of PVA/SA@ZIF-8, with the composites generally performing better at higher temperatures. However, the extent of improvement varies across treatments, with Figure 9 C showing the greatest increase. This suggests that optimizing temperature could be a valuable strategy to enhance the removal efficiency of this composite in dye-removal applications. Further studies, including kinetic and thermodynamic analyses, would be beneficial for understanding the underlying mechanisms of temperature-dependent behavior.

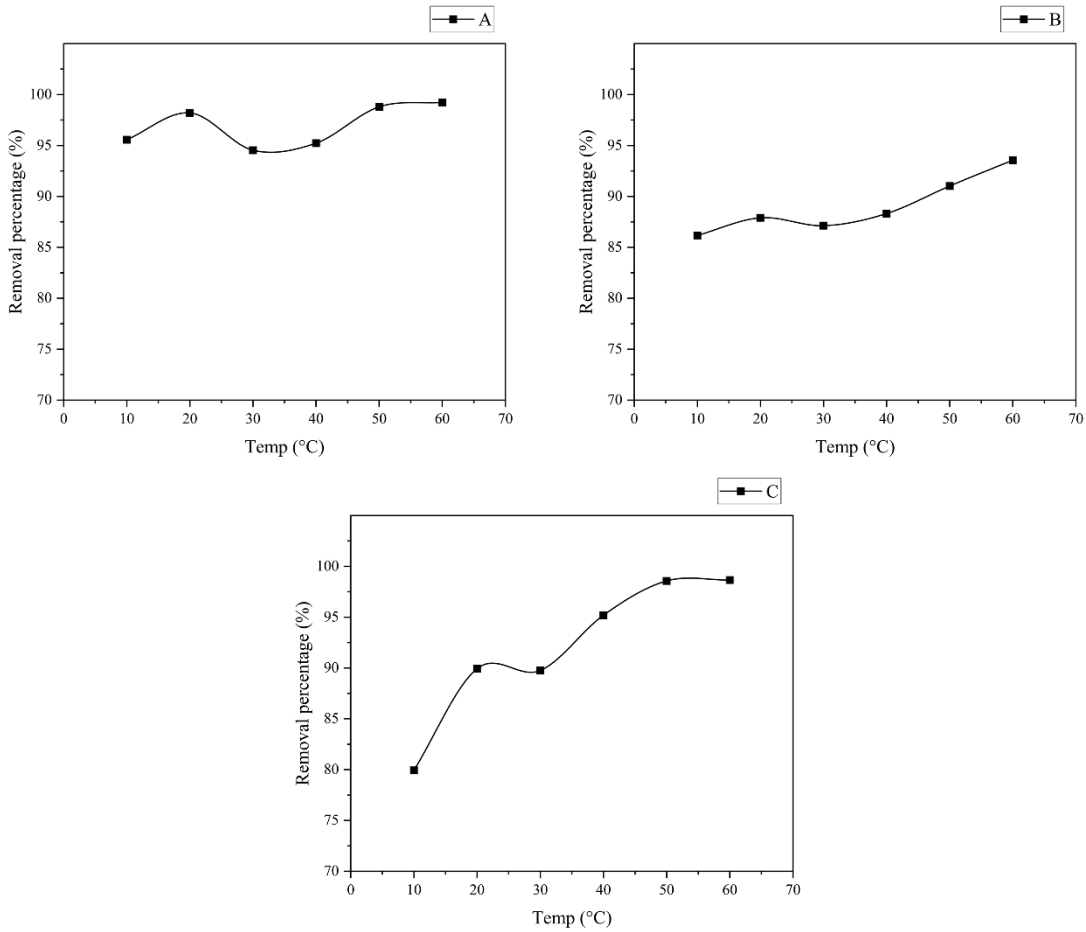

Figure 9: Effect of temperature on the removal curve of PVA/SA@ZIF-8 hydrogels synthesized using (A) one-step in-situ preparation, (B) two-step in-situ preparation, and (C) direct mixing of MOF into the hydrogel.

3.2.4. Effect of the initial concentration on removal efficiency

The removal percentages of PVA/SA@ZIF-8 hydrogel beads were measured in 20 mL of basic violet dye solution with concentrations of 1, 2.5, 5, 10, 15, and 20 mg/L, with a constant amount of 0.02 g of adsorbent, for 90 min at room temperature.

The effect of the initial dye concentration on the removal efficiency of basic violet by PVA/SA@ZIF-8 was investigated, and the results are shown in Figure 10. In all cases, the removal percentage decreased with increasing concentration, a common phenomenon in adsorption processes, which is indeed due to the saturation of available adsorption sites. Among the methods, method B exhibited superior performance, achieving a maximum removal efficiency of approximately 69 % at low concentrations. Methods A and C exhibit a significant drop in efficiency at higher concentrations, falling below 15 %. Sample B also demonstrated greater stability across the mid-concentration range, indicating enhanced adsorption capacity and potential for practical application under varying contaminant loads.

3.2.5. Effect of time on removal efficiency

In the last step of the removal efficiency study, 0.02 g of PVA/SA@ZIF-8 hydrogel beads were stirred in 20 mL of a basic violet dye solution at 10 mg/L for 10, 20, 30, 50, 70, 90, and 120 min at room temperature [35].

As shown in Figure 11, the removal efficiency of basic violet dye by PVA/SA@ZIF-8 hydrogels increases over time, with all three graphs (A, B, and C) demonstrating near-maximal removal (~90 %) at 120 min. Graphs A and C indeed suggest a gradual adsorption process in which dye molecules progressively occupy available adsorption sites, leading to a slow but steady increase in efficiency. In contrast, Graph B demonstrates an initial rapid adsorption phase followed by a stabilization period, indicating a fast initial uptake rate of the dye.

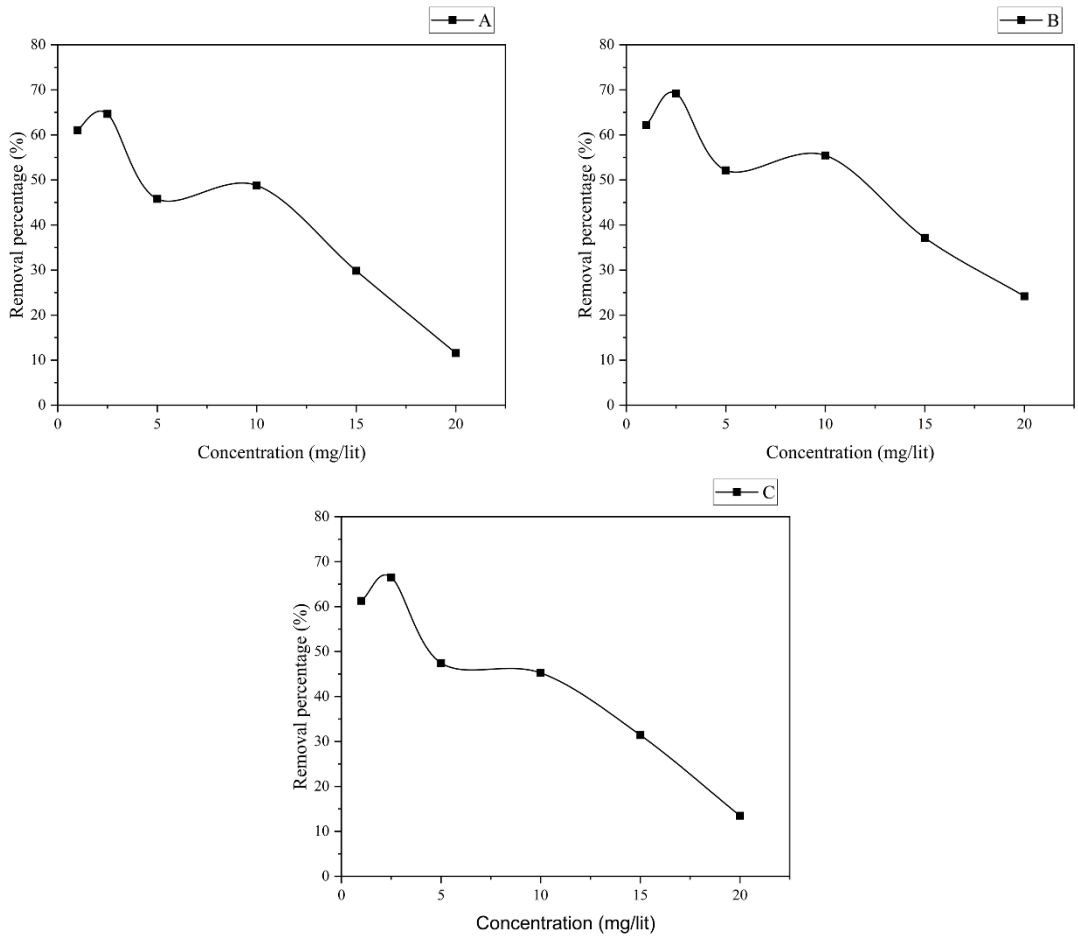

Figure 10: Effect of initial concentration on the removal curve of PVA/SA@ZIF-8 hydrogels synthesized using (A) one-step in-situ preparation, (B) two-step in-situ preparation, and (C) direct mixing of MOF into the hydrogel.

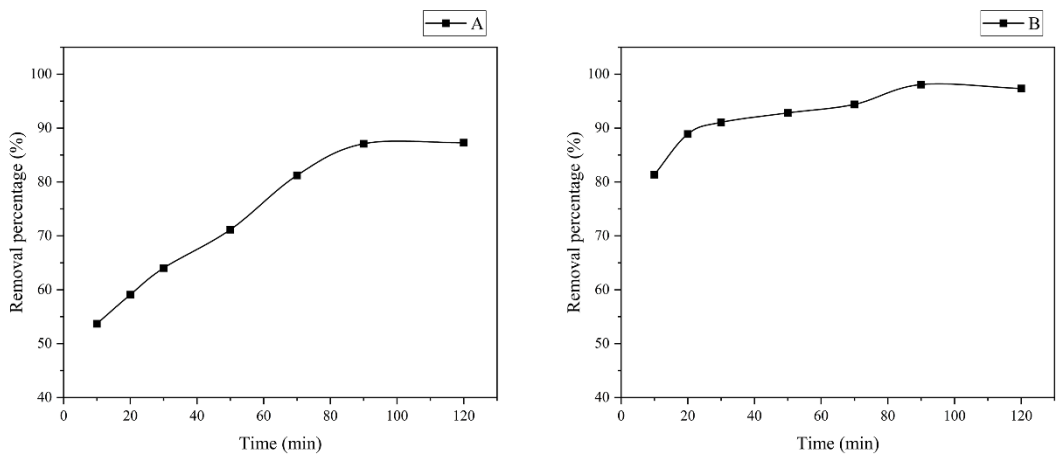

Figure 11: Effect of time on the removal curve of PVA/SA@ZIF-8 hydrogels synthesized using (A) one-step in-situ preparation, (B) two-step in-situ preparation, and (C) direct mixing of MOF into the hydrogel.

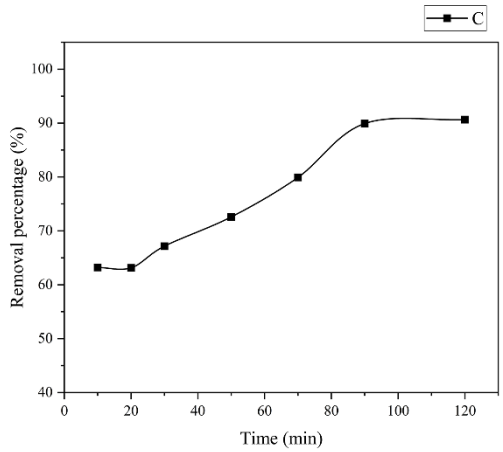

Figure 11: Continue

3.2.6. Performance evaluation of synthesized adsorbents under optimized conditions

The adsorption performance of various synthesized adsorbents was evaluated under optimized conditions: 20 mg adsorbent dose, 20 mL solution volume, 90 min contact time, 20 °C temperature, and pH 12. The initial dye concentration was fixed at 10 mg/mL using basic violet as the model contaminant.

The extent of dye removal was indirectly assessed by UV-Vis spectroscopy, measuring the residual dye concentration in solution. In Figure 12, all spectra exhibited a characteristic absorbance peak of basic violet around 550 nm. A lower absorbance at this wavelength corresponds to higher dye removal efficiency.

Among the tested samples, the synthesized composite prepared via the two-step in situ method (sample B) showed the highest dye removal, as evidenced by the lowest absorbance at 550 nm. In a study comparing dye uptake, pure ZIF-8 demonstrated superior performance compared to both the PVA/SA polymer matrix and other ZIF-8 composite materials (samples B & C). This suggests that ZIF-8's inherent properties, like its porous structure, contribute significantly to dye adsorption. The one-step in situ composite (sample A) and the direct mixed composite (sample C) displayed moderate removal efficiencies, whereas the polymeric blend without MOF (PVA/SA) exhibited relatively weak adsorption capacity.

The findings highlight that both the presence of ZIF-8 and the method of its incorporation into the polymer matrix significantly influence the adsorption behavior. The enhanced performance of sample B, synthesized using a two-step in situ method, suggests that this approach may improve the distribution and interaction of ZIF-8 particles within the hydrogel, thereby increasing the availability of adsorption sites.

3.2.7. Kinetic modeling of adsorption

In this study, the adsorption kinetics of three systems were evaluated using various kinetic models to determine the most suitable mechanism governing adsorption. Initially, the widely employed pseudo-first-order (PFO) and pseudo-second-order (PSO) kinetic models, along with the Langmuir kinetic model, were applied to the experimental data.

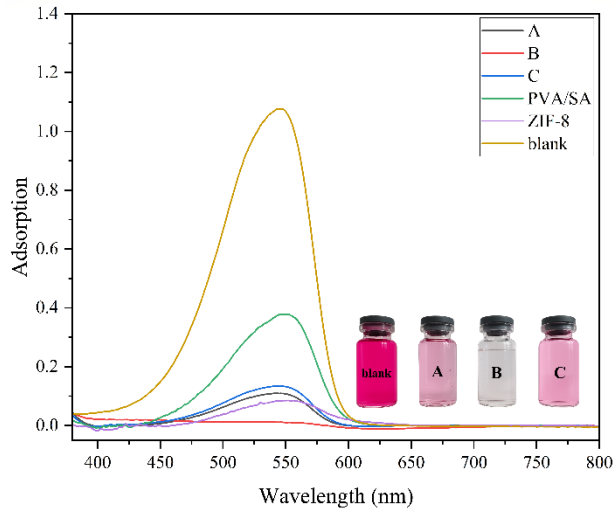

Figure 12: The absorption spectrum of basic violet color by PVA/SA@ZIF-8 hydrogels, synthesized using (A) One-step in-situ preparation, (B) Two-step in-situ preparation, and (C) Direct mixing of MOF into the hydrogel, along with ZIF-8 MOF and PVA/SA matrix.

The pseudo-first-order (PFO) kinetic model is based on the assumption that the rate of occupation of adsorption sites is proportional to the number of unoccupied sites (Eq. 1):

$$q_t = q_e(1 - e^{-k_1 t}) \quad (1)$$

- q_t: amount of adsorbate adsorbed at time t (mg/g)
- q_e: equilibrium adsorption capacity (mg/g)
- k_1: rate constant of pseudo-first-order model (1/min)
- t: time (min)

The pseudo-second-order (PSO) model assumes that the adsorption process follows chemisorption involving electron sharing or exchange (Eq. 2):

$$q_t = \frac{k_2 q_e^2 t}{1 + k_2 q_e t} \quad (2)$$

- k_2: rate constant of pseudo-second-order model (g/mg.min)

The Langmuir kinetic model, based on the Langmuir isotherm theory, assumes monolayer adsorption without interaction between adsorbed molecules (Eq. 3):

$$q_t = \frac{q_e k_L t}{1 + k_L t} \quad (3)$$

- k_L: Langmuir rate constant (1/min)

In all three synthesis methods, the pseudo-second-order (PSO) model better represents the adsorption process of basic violet dye onto the PVA/SA@ZIF-8 hydrogel composite than the pseudo-first-order (PFO) model, indicating that chemisorption is the dominant mechanism (Figure 13). The PSO model's superior fit, as indicated by higher R^2 values, suggests that electron sharing or transfer between dye molecules and the hydrogel's active sites is the primary driver of the adsorption rate, rather than simple physical interactions described by the PFO model.

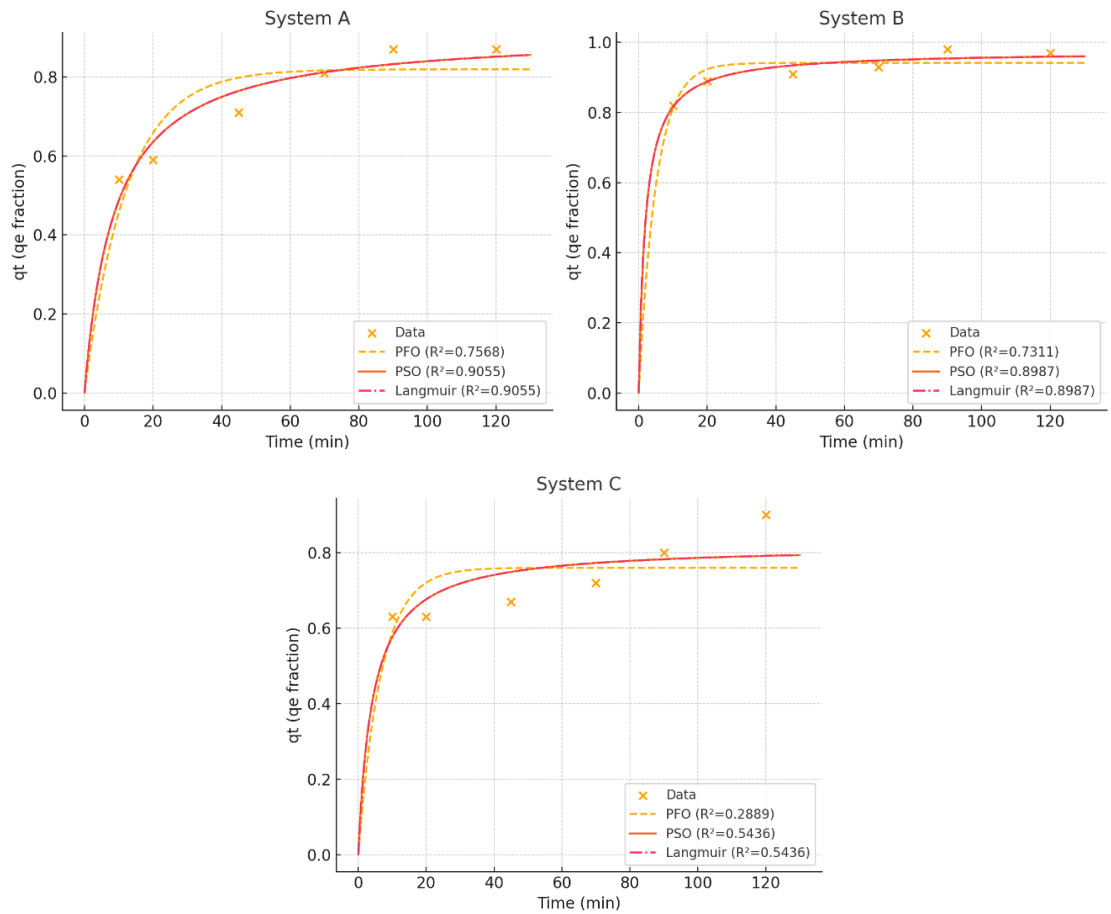

Figure 13: Adsorption kinetics for PVA/SA@ZIF-8 hydrogels, synthesized by (A) One-step in-situ preparation, (B) Two-step in-situ preparation, and (C) Direct mixing of MOF in hydrogel methods, comparing PFO, PSO, and Langmuir models.

Additionally, the Langmuir model, which assumes monolayer adsorption on a homogeneous surface, and the PSO model, often indicative of chemisorption, both provide good fits, implying a combination of both chemisorption and monolayer formation in the overall adsorption mechanism.

System A, synthesized using a one-step, in-situ method, demonstrates a high affinity for basic violet dye adsorption. The data fit best to the pseudo-second-order (PSO) model (R^2 = 0.9055), indicating that the adsorption process follows a chemisorption mechanism. A similar R^2 value for the Langmuir model (0.9055) suggests effective integration of ZIF-8 MOF within the hydrogel, resulting in a uniform and accessible surface. This suggests that the dye molecules form a monolayer on the well-dispersed ZIF-8 sites within the hydrogel.

In the two-step in-situ synthesis (system B), the pseudo-second-order (PSO) model best described the dye removal kinetics (R^2 = 0.8987), indicating chemisorption as the primary mechanism. The Langmuir model yielded an R^2 value of 0.8997, nearly identical to that of the Langmuir model, suggesting that the adsorbent produced is both highly effective and uniform. This strong correlation implies that the formation of a chemical bond or interaction between the dye and the MOF active sites is the rate-determining step, resulting in monolayer coverage of the dye on the surface.

System C (Direct mixing of MOF) yielded an adsorbent with lower overall kinetic performance, as evidenced by lower R^2 values across all models. However, the PSO model (R^2 = 0.5436) still provided a better fit than the PFO model (R^2 = 0.2889), suggesting that, despite this less effective synthesis, chemisorption remains the primary kinetic mechanism. The Langmuir model also gave an identical R^2 value of 0.5436. The lower R^2 values in this system, compared to systems A and B, are likely due to the direct mixing method, which may result in non-uniform dispersion or aggregation of ZIF-8 MOF particles within the hydrogel. This would result in fewer accessible active sites and a less-defined adsorption pathway, but the underlying mechanism still appears to be a chemisorption-controlled process approaching monolayer saturation.

Generally, the adsorption of basic violet dye onto PVA/SA@ZIF-8 hydrogels is primarily governed by a chemisorption mechanism, as demonstrated by the strong fit of the pseudo-second-order kinetic model. This chemisorption process likely leads to the formation of a monolayer of dye molecules on the hydrogel-MOF composite surface, as supported by the good fit of the Langmuir model. In simpler terms, this means the dye molecules bind to the hydrogel-MOF material via chemical bonds, forming a single surface layer rather than multiple layers. The good fit of these models indicates a strong preference for chemisorption and monolayer formation. The synthesis method significantly impacts overall adsorption performance, with in-situ methods (systems A & B) yielding materials with a more uniform distribution of active sites, leading to a more pronounced, well-defined chemisorption process and higher R^2 values. In contrast, the direct mixing method (system C) results in a less ideal adsorbent.

To gain a deeper understanding of adsorption behavior, especially in systems with surface heterogeneity or internal diffusion limitations, the Elovich and intraparticle diffusion models were used.

The Elovich model is commonly used for chemisorption on highly heterogeneous surfaces (Eq. 3):

$$q_t = \frac{1}{\beta}\ln(1 + \alpha\beta t) \quad (4)$$

- α: initial adsorption rate (mg/ g.min)
- β: desorption constant related to surface coverage (g/mg)

The intraparticle diffusion model [36], developed by Weber and Morris, describes the diffusion of adsorbate molecules into the pores of the adsorbent:

$$q_t = k_{id}t^{1/2} + C \quad (5)$$

The adsorption kinetics shown in Figure 14 indicate that the Elovich model fits the experimental data well, particularly in systems A and B. This suggests surface heterogeneity and varying adsorption activation energies. Conversely, the intraparticle diffusion model, which considers diffusion-controlled processes within porous adsorbents, more accurately describes the kinetics of system C. In this case, pore diffusion seems to be the primary rate-limiting step.

According to the R^2 values in Table 1, the Elovich model provided a strong fit for systems A (R^2 = 0.9690) and B (R^2 = 0.9289). This indicates a close alignment with the experimental data and suggests that surface heterogeneity and variable activation energies are

Table 1: R^2 values for the Elovich and Intra Diffusion models applied to Samples (A) One-step in-situ preparation, (B) Two-step in-situ preparation, and (C) Direct mixing of MOF in hydrogel methods, demonstrating the model fitting performance for each system.

Model	System A	System B	System C
Elovich (R^2)	0.9690	0.9289	0.7465
Intra Diffusion (R^2)	0.9691	0.8935	0.8695

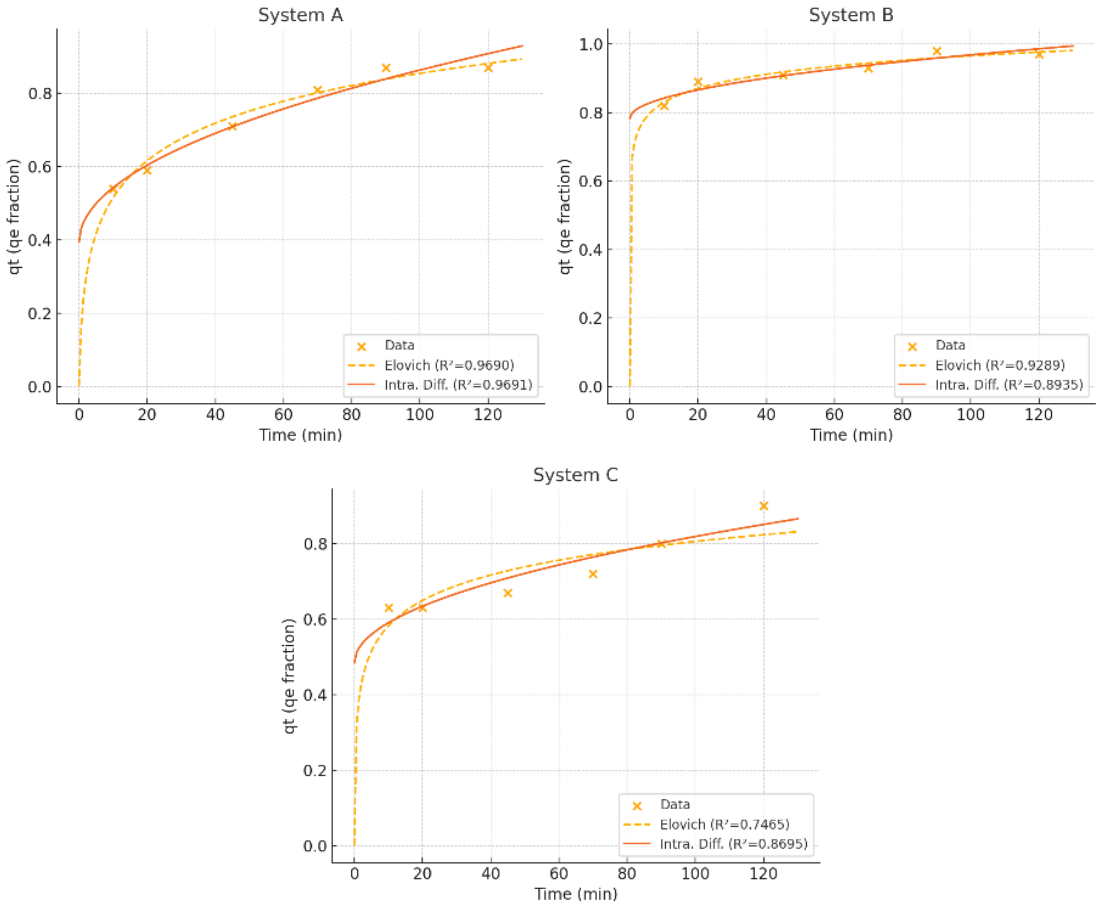

Figure 14: Adsorption kinetics for PVA/SA@ZIF-8 hydrogels, synthesized by (A) One-step in-situ preparation, (B) Two-step in-situ preparation, and (C) Direct mixing of MOF in hydrogel methods, comparing Elovich and Intraparticle Diffusion models.

significant factors in these samples. In contrast, for system C, the Elovich model yielded an R^2 of 0.7465, indicating a poor fit and underscoring its limitations in accurately describing the system's kinetics.

The Intra Diffusion model showed similarly high R^2 values across systems A and B (0.9691 and 0.8935, respectively), which further supports its relevance for describing diffusion-controlled adsorption processes in these systems. System C, however, showed a slightly better fit with the intra-diffusion model (R^2 = 0.8695) than with the Elovich model, suggesting that pore diffusion may be the rate-limiting step in this system, consistent with the observed diffusion-controlled behavior.

The detailed kinetic analysis using Elovich and Intraparticle Diffusion models reveals that the adsorption mechanism, specifically the rate-limiting step, is dictated by the synthesis method of hydrogel-MOF composites. While chemisorption is the primary mechanism for all systems (as indicated by PSO model fit), in-situ prepared systems (A & B) exhibit a combination of chemisorption and intraparticle diffusion, whereas the less effective direct mixing method (system C) is dominated by intraparticle diffusion. This high-

lights how synthesis influences the composite's physical structure and subsequently, the adsorption kinetics.

3.2.8. Thermodynamic modeling of adsorption

To gain a deeper understanding of the adsorption behavior of PVA/SA@ZIF-8 hydrogels synthesized by different methods, we evaluated their thermodynamic parameters. We calculated the standard Gibbs free energy change (ΔG°), enthalpy change (ΔH°), and entropy change (ΔS°) using specific thermodynamic equations (Eqs. 6 and 7):

$$\frac{\Delta H^\circ}{RT} - \frac{\Delta S^\circ}{R} = \ln K \quad (6)$$

$$T\Delta S^\circ - \Delta H^\circ = \Delta G^\circ \quad (7)$$

Where K is the equilibrium constant, R is the universal gas constant (8.314 J/mol.K), and T is the absolute temperature in Kelvin. The values of ΔH^0, ΔS^0 and and ΔG^0 at 298 K for each sample are summarized in Table 2.

The positive enthalpy change (ΔH°) values for all samples indicate that the adsorption of the dye onto the PVA/SA@ZIF-8 hydrogels is endothermic. Sample C exhibited the highest ΔH° (+47.86 kJ/mol), suggesting a stronger temperature dependence and requiring more energy for adsorption, while sample A has the lowest ΔH° (+11.72 kJ/mol). The positive entropy changes (ΔS°) observed during adsorption indicate an increase in disorder at the solid-solution interface as dye molecules interact with the adsorbent. This can be attributed to the structural changes and potential desolvation of dye molecules as they bind to the surface. Sample C, with the highest ΔS°, suggests greater structural disruption than the other samples.

Gibbs free energy (ΔG°) values were negative at 298 K, confirming that the adsorption processes were spontaneous under the studied conditions. Sample B had the most favorable spontaneity with ΔG° = -3.96 kJ/mol. The magnitude of ΔG° values between 0 and -20 kJ/mol suggests that the dye adsorption onto these composites is primarily a physical adsorption process. The Van't Hoff plots (ln K vs. 1/T) showed good linearity (Figure 15), further confirming the validity of the thermodynamic approach.

Table 2: Thermodynamic parameters of PVA/SA@ZIF-8 composites.

Synthesis Method	ΔG^0 (kJ/mol) at 298 K	ΔS° (J/mol.K)	ΔH° (kJ/mol)	Sample
One-step in-situ	-0.38	40.61	11.72	A
Two-step in-situ	-3.96	86.63	21.85	B
Direct mixing	-1.16	164.49	47.86	C

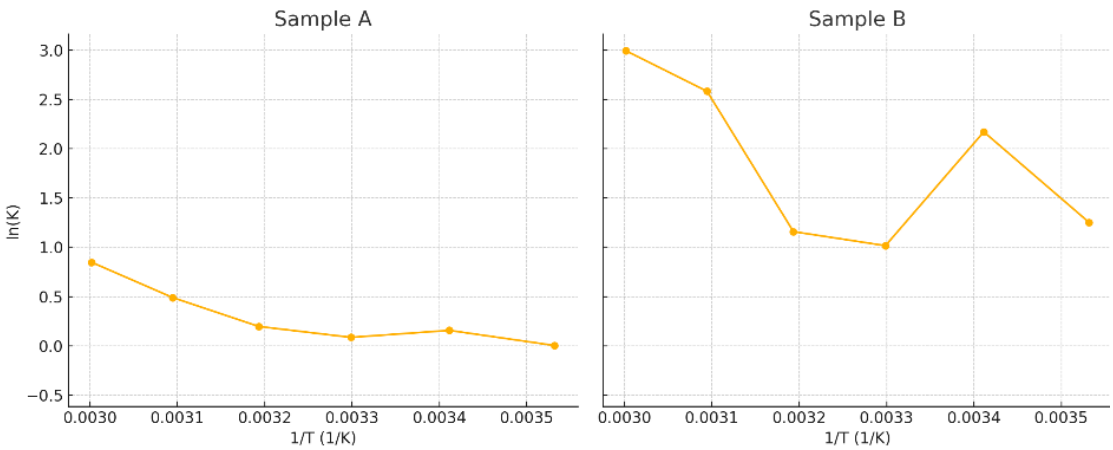

Figure 15: Van't Hoff Plots for PVA/SA@ZIF-8 composites , synthesized by (A) One-step in-situ preparation, (B) Two-step in-situ preparation, and (C) Direct mixing of MOF in hydrogel methods.

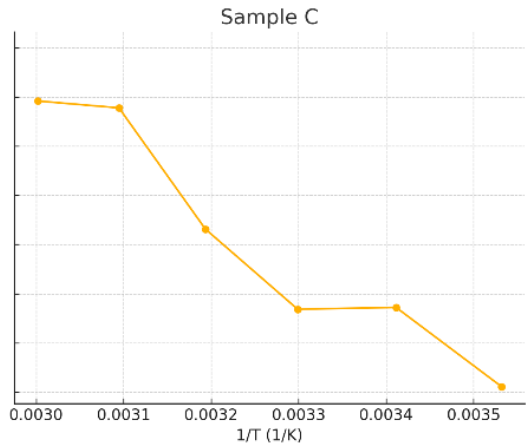

Figure 15: Continue.

The thermodynamic study indicates that all three PVA/SA@ZIF-8 composites exhibit spontaneous, endothermic adsorption of a dye. However, the two-step in-situ-synthesized sample (sample B) exhibited the most favorable thermodynamic performance, suggesting that this method is the most effective for promoting dye adsorption under the studied conditions. This means that while all the materials are capable of adsorption, sample B is the most efficient.

4. Conclusions

In this study, polyvinyl alcohol/sodium alginate (PVA/SA) hydrogel composites incorporating ZIF-8 metal–organic frameworks (MOFs) were successfully synthesized using three distinct approaches-one-step in situ, two-step in situ, and direct mixing-to elucidate the role of synthesis methodology on structural integration and adsorption efficiency. Comprehensive physico-chemical characterization (FESEM, EDS, XRD, FTIR, and DLS) confirmed the successful incorporation of ZIF-8 within the biopolymer matrix and revealed distinct morphological and interfacial characteristics across synthesis routes. Among the investigated systems, the two-step in-situ method demonstrated superior performance, attributed to optimal interfacial interaction and homogeneous dispersion of ZIF-8 nanocrystals within the polymeric network. The resulting hydrogel exhibited nearly complete Basic Violet dye removal (≈ 99 %) under optimized conditions (pH = 12, 60 °C, 20 mg adsorbent, 90 min contact time), with sustained efficiency even at low dye concentrations (≈ 69% removal at 5 mg L^{-1}). Kinetic analysis revealed that adsorption followed the pseudo-second-order (PSO) model ($R^2 \approx 0.99$), indicative of chemisorptive interactions, while the intraparticle diffusion model identified multi-stage diffusion behavior, particularly in more compact morphologies. Thermodynamic parameters ($\Delta G° = -3.96$ kJ mol^{-1}; $\Delta H° = +21.85$ kJ mol^{-1}; $\Delta S° = +86.63$ J mol^{-1} K^{-1}) confirmed that the adsorption process was spontaneous and endothermic, reflecting increased molecular randomness and enhanced dye–adsorbent affinity at elevated temperatures. FTIR spectral shifts (O–H and C–O–Zn) further evidenced chemical coordination between ZIF-8 and hydroxyl functionalities, strengthening the composite structure and stability. Overall, the results establish that the synthesis route governs MOF spatial distribution, interfacial chemistry, and porosity, which collectively dictate adsorption kinetics and thermodynamics. The two-step in-situ synthesis emerges as a technologically and environmentally advantageous approach, offering an efficient, scalable pathway for producing high-performance MOF–biopolymer hybrid adsorbents for industrial wastewater treatment and sustainable environmental remediation. Future work should focus on adsorption isotherm modeling, recyclability assessment, and multi-contaminant removal studies, enabling a deeper understanding of the underlying mechanisms and expanding potential applications toward real-world effluent purification and advanced functional material design.

5. References

1. Brusko V, Artur K, Aydar R, Dimiev AM. Unraveling the infrared spectrum of graphene oxide. Carbon. 2024; 229:119507-7. https://doi.org/10.1016/j.carbon.2024.119507.
2. Wang H, Pei X, Kalmutzki M, Yang J, Yaghi OM. Large cages of zeolitic imidazolate frameworks. Account Chem Res. 2022; 55(5):707-21. https://doi.org/10.1021/acs.accounts.1c00740.
3. Kumar A, Sood A, Sung Soo Han. Poly (vinyl alcohol)-alginate as potential matrix for various applications: A focused review. Carbohydrate Polym. 2022; 277:118881-1. https://doi.org/10.1016/j.carbpol.2021. 118881.
4. Wang T, Lin J, Chen Z, Megharaj M, Naidu R. Green synthesized iron nanoparticles by green tea and eucalyptus leaves extracts used for removal of nitrate in aqueous solution. J Clean Prod. 2014; 83:413-9. https://doi.org/10.1016/j.jclepro.2014.07.006.
5. Tran NH, Reinhard M, Gin KYH. Occurrence and fate of emerging contaminants in municipal wastewater treatment plants from different geographical regions-a review. Water Res. 2018; 133:182-207. https://doi.org/10.1016/j.watres.2017.12.029.
6. Simon-Yarza T, Mielcarek A, Couvreur P, Serre C. Nanoparticles of metal-organic frameworks: on the road to in vivo efficacy in biomedicine. Adv Mater. 2018; 30(37):1707365. https://doi.org/10.1002/adma.201707365.
7. Goudarzi S, Gharanjig K, Kazemian H, Ghasemi E, Imani H, Gharanjig H. Enhanced removal of cochineal dye from textile effluents using MIL 53(Al): optimization, kinetics, and thermodynamic studies. Prog Color Colorant Coat. 2025;18(1):1-16. https://doi.org/10.30509/pccc.2024.167297.1289.
8. Barakat A, Ennaji W, Krimissa S, Bouzaid M. Heavy metal contamination and ecological-health risk evaluation in peri-urban wastewater-irrigated soils of Beni-Mellal city (Morocco). Int J Environ Health Res. 2020;30(4):372-87. https://doi.org/10.1080/09603123.2019.1595540.
9. Shakir M, Azahari B, Yusup Y, Yhaya M, Salehabadi A, Ahmad MI. Preparation and characterization of mycelium as a bio-matrix in fabrication of bio-composite. J Adv Res Fluid Mech Therm Sci. 2024; 65(2):253-263.
10. Lee Y, Jang MS, Cho H, Kwon H, Kim S, Ahn W. ZIF 8: A comparison of synthesis methods. Chem Eng J. 2015;271:276-80. https://doi.org/10.1016/j.cej.2015.02.094.
11. Veghari Atigh F, Shaki H. Cost-effective removal of methylene blue dye from wastewater using polyacrylamide/sodium carboxymethyl cellulose/ magnetic halloysite nanotube hydrogel. Int J Environ Sci Technol. 2025; 22:9849-76. https://doi.org/10.1007/s13762-025-06461-x.
12. Tristan JK, Slowinski IA, Dao B, Cortez VH, Gredig T. Zeta potential and size analysis of zeolitic imidazolate framework 8 nanocrystals prepared by surfactant-assisted synthesis. Langmuir. 2024;40:6138-6148. https://doi.org/10.1021/acs.langmuir.3c03193.
13. Shaki H. Removal of methylene blue and maxilon blue dyes using a polyvinyl alcohol/poly(acrylic acid co acrylamide) composite hydrogel from water. Pigm Resin Technol. 2023;52:521-31. https://doi.org/10.1108/PRT-11-2021-0130.
14. Sutar P, Rao Bakuru V, Yadav P, Laha S, Babu Kalidindi S, Kumar Maji T. Nanocomposite hydrogel of Pd@ZIF 8 and Laponite®: Size selective hydrogenation catalyst under mild conditions. Chem. 2020;27:3268-3272. https://doi.org/10.1002/chem.20 200 4345.
15. Li Y, Wen J, Xue Z, Yin X, Yuan L, Yang C. Removal of Cr(VI) by polyaniline embedded polyvinyl alcohol/sodium alginate beads: Extension from water treatment to soil remediation. J Hazard Mater. 2022; 426:127809. https://doi.org/10.1016/j.jhazmat.2021.127809.
16. Baigorria E, Cano LA, Sanchez LM, Alvarez VA, Ollier RP. Bentonite composite polyvinyl alcohol/ alginate hydrogel beads: Preparation, characterization and their use as arsenic removal devices. Environ Nanotechnol Monit Manag. 2020;14:100364. https://doi.org/10.1016/j.enmm.2020.100364.
17. Jang J, Lee D. Enhanced adsorption of cesium on PVA alginate encapsulated Prussian blue graphene oxide hydrogel beads in a fixed bed column system. Bioresour Technol. 2016; 218:294-300. https://doi.org/10.1016/j.biortech.2016.06.100.
18. Gwon K, Han I, Lee S, Kim Y, Lee D. Novel metal–organic framework based photocrosslinked hydrogel system for efficient antibacterial applications. ACS Appl Mater Interfaces. 2020; 12:20234-42. https://doi.org/10.1021/acsami.0c03187.
19. Li J, Wang X, Zhao G, Chen C, Chai Z, Alsaedi A. Metal–organic framework based materials: Superior adsorbents for the capture of toxic and radioactive metal ions. Chem Soc Rev. 2018; 47(7):2322-56. https://doi.org/10.1039/C7CS00543A.
20. Zhu L, Zong L, Wu X, Li M, Wang H, You J, Li C. Shapeable fibrous aerogels of metal–organic frameworks templated with nanocellulose for rapid and large capacity adsorption. ACS Nano. 2018; 12 (5):4462-68. https://doi.org/10.1021/acsnano.8b00566.
21. Ahmed I, Jhung SH. Composites of metal-organic frameworks: Preparation and application in adsorption. Mater Today. 2014;17(3):136-146. https://doi.org/10.1016/j.mattod.2014.03.002.
22. Zhang G, Chen H, Yang G, Fu H. Preparation of in situ ZIF 9 grown on sodium alginate/polyvinyl alcohol hydrogels for enhancing Cu(II) adsorption from aqueous solutions. J Inorg Organomet Polym Mater. 2022; 32:4576-4588. https://doi.org/10.1007/s10904-022-02463-1.
23. Phu NAMM, Wi E, Jeong G, Kim H, Singha NR, Chang M. Highly efficient dye adsorption by

hierarchical porous SA/PVA/ZIF 8 composite microgels prepared via microfluidics. Carbohydr Polym. 2025; 350:123016. https://doi.org/10.1016/j.carbpol.2024.123016.
24. Ta DN, Nguyen HKD, Trinh BX, Le QT, Ta HN, Nguyen HT. Preparation of nano ZIF 8 in methanol with high yield. Can J Chem Eng. 2018; 96(7):1518-31. https://doi.org/10.1002/cjce.23155.
25. Akhundzadeh Tezerjani A, Halladj R, Askari S. Different view of solvent effect on the synthesis methods of zeolitic imidazolate framework 8 to tuning the crystal structure and properties. RSC Adv. 2021; 11:19914-23. https://doi.org/10.1039/D1RA02856A.
26. Zhang X, Lin B, Zhao K, Wei J, Guo J, Cui W. A free standing calcium alginate/polyacrylamide hydrogel nanofiltration membrane with high anti fouling performance: Preparation and characterization. Desalination. 2015;365:234-241. https://doi.org/10.1016/j.desal.2015.03.015.
27. Pan Y, Liu Y, Zeng G, Zhao L, Lai Z. Rapid synthesis of zeolitic imidazolate framework 8 (ZIF 8) nanocrystals in an aqueous system. Chem Commun. 2011; 47(7):2071-2073. https://doi.org/10.1039/C0CC05002D.
28. Zhang X, Li Z, Zhang T, Chen J, Jib W, Wei Y. Fabrication of an efficient ZIF 8 alginate composite hydrogel material and its application to enhanced copper(II) adsorption from aqueous solutions. New J Chem. 2021;45:15876-86. https://doi.org/10.1039/D1NJ03427H.
29. Wang X, Chen X, Yoon K, Fang D, Hsiao BS, Chu B. High flux filtration medium based on nanofibrous substrate with hydrophilic nanocomposite coating. Environ Sci Technol. 2006; 40(5):1724-30. https://doi.org/10.1021/es050512j.
30. Senapati S, Giri J, Mallick L, Singha D, Bastia TK, Rath P, et al. Rapid adsorption of industrial cationic dye pollutant using base activated rice straw biochar: performance, isotherm, kinetic and thermodynamic evaluation. Discov Sustain. 2025; 46(6):1-24. https://doi.org/10.1007/s43621-025-00835-4.
31. Hadi A, Karimi Sabet J, Dastbaz A. Parametric study on the mixed solvent synthesis of ZIF 8 nano and micro particles for CO adsorption: A response surface study. Front Chem Sci Eng. 2018; 12(4):713-22. https://doi.org/10.1007/s11705-018-1770-3.
32. Hao C, Zhou D, Xu J, Hong S, Wei W, Zhao T. One pot synthesis of vancomycin encapsulated ZIF 8 nanoparticles as multivalent and photocatalytic antibacterial agents for selective killing of pathogenic gram positive bacteria. J Mater Sci. 2021;56(15): 9434-9444. https://doi.org/10.1007/s10853-021-05828-y.
33. Santhosh S, Jha CB, Singh C, Kumar R, Pandey NK, Varshney R, et al. Preparation and evaluation of physically cross linked hydrogel of tranexamic acid. AIP Conf Proc. 2023; 2800:020161. https://doi.org/10.1063/5.0163649.
34. Wang P, Tan L, Yuan G, Feng S, Tang H, Wang G. ZIF 8 modified polyvinyl alcohol/chitosan composite aerogel for efficient removal of Congo red. J Solid State Chem. 2022; 316:123628. https://doi.org/10.1016/j.jssc.2022.123628.
35. Deng Y, Mao Q, Luo S, Xie X, Luo L. Adsorption based removal of Sb(III) from wastewater by graphene oxide modified zirconium based metal–organic framework composites. Adsorpt Sci Technol. 2022; 2:105321. https://doi.org/10.1155/2022/9222441.
36. Wu FC, Tseng RL, Juang RS. Initial behavior of intraparticle diffusion model used in the description of adsorption kinetics. Chem Eng J. 2009; 153:1-8. https://doi.org/10.1016/j.cej.2009.04.042.

How to cite this article:
Moradi J, Alikhah Shirayeh A, Aram E, Shaki H. Investigation of the Distribution and Placement of Metal-Organic Frameworks in Polyvinyl Alcohol/Sodium Alginate Composites and Their Effects on Adsorption Properties for Dye Removal: A Comparison of Different Synthesis Methods. Prog Color Colorants Coat. 2026;19(3):329-350. https://doi.org/10.30509/pccc.2025.167568.1403.